Published in final edited form as:
Int J Radiat Oncol Biol Phys. 2014 September 1; 90(1): 155–163. doi:10.1016/j.ijrobp.2014.05.041.

FAT COMPOSITION CHANGES IN BONE MARROW DURING CHEMOTHERAPY AND RADIOTHERAPY

Ruben Carmona, M.D., M.A.S.[*], **Jakub Pritz, Ph.D.**[*], **Mark Bydder, Ph.D.**[†], **Sachin Gulaya, B.S.**[*], **He Zhu, M.D., Ph.D.**[*], **Casey W. Williamson, B.A.**[*], **Christian S. Welch, M.D.**[†], **Florin Vaida, Ph.D.**[‡], **Graeme Bydder, M.D.**[†], and **Loren K. Mell, M.D.**[*]

[*] Department of Radiation Medicine and Applied Sciences, University of California San Diego, La Jolla, CA

[†] Department of Radiology, University of California San Diego Medical Center, San Diego, CA

[‡] Department of Family and Preventive Medicine, Biostatistics and Bioinformatics, University of California San Diego Medical Center, San Diego, CA

Abstract

Purpose/Objectives(s)—To quantify changes in bone marrow fat fraction and determine associations with peripheral blood cell counts.

Methods and Materials—In this prospective study, 19 patients received either highly myelotoxic (radiotherapy plus cisplatin, 5FU/MMC or cisplatin/5FU/cetuximab) or less myelotoxic treatment (capacitabine-radiotherapy or no concurrent chemotherapy). Patients underwent MR imaging and venipuncture at baseline, mid-treatment, and post-treatment visits. We performed mixed effects modeling of the mean proton density fat fraction (PDFF(%)) by linear-time, treatment, and vertebral column region (L4-S2 vs. T10-L3 vs. C3-T9), while controlling for cumulative mean dose and other confounders. Spearman rank correlations were performed by blood cell counts versus the difference in PDFF(%) pre- and post-treatment.

Results—Cumulative mean dose was associated with a 0.43% per Gy (p=.004) increase in PDFF(%). In the highly myelotoxic group, we observed significant changes in PDFF(%) per visit within L4-S2 (10.1%,p<.001) and within T10-L3 (3.93%,p=.01), relative to the reference C3-T9. In the less myelotoxic group, we did not observe significant changes in PDFF(%) per visit according to region. Within L4-S2, we observed a significant difference between treatment groups in the change in PDFF(%) per visit (5.36%,p=.04). Rank correlations of the inverse log difference in WBC versus the difference in PDFF(%) overall and within T10-S2 ranged from 0.69-0.78 (p<0.05). Rank correlations of the inverse log difference in ANC versus the difference in PDFF(%) overall and within L4-S2 ranged from 0.79-0.81 (p<0.05).

Corresponding Author: Loren K. Mell, M.D. Department of Radiation Medicine and Applied Sciences 3855 Health Sciences Drive, MC0843 La Jolla, CA 92093 lmell@ucsd.edu/ (858) 246-0471/ fax (858) 822-5568.

Disclosures:
The sponsors had no role in the preparation of this manuscript.

Conclusion—MRI fat quantification is sensitive to marrow composition changes that result from (chemo)radiotherapy. These changes are associated with peripheral blood cell counts. This study supports a rationale for bone marrow sparing treatment planning to reduce the risk of hematologic toxicity.

INTRODUCTION

A limiting factor in cancer treatment with chemoradiotherapy is marrow toxicity (1,2). Bone marrow is composed of red and yellow marrow. Red marrow consists of hematopoietic stem cells that produce erythrocytes, leukocytes, and thrombocytes. Yellow marrow, like red marrow, contains abundant capillaries, but is not directly involved in hematopoiesis. The stroma of the reticular network of yellow marrow is primarily filled with lipids, thus exhibiting a higher fat content. Red marrow is found in flat bones including the pelvis, sternum, and vertebrae, while yellow marrow is found in the medullary cavities of long bones. Chemotherapy and radiation both suppress the hematopoietic system, leading to a reduction in red marrow and an increase in yellow marrow (3). This composition change can result in neutropenia and thrombocytopenia that require chemotherapy dose reductions and delays thus compromising treatment outcomes (4,5).

T1-weighted magnetic resonance imaging (MRI) provides a qualitative impression of the amount of fat present in bone marrow due to the short T1 of fat compared to other tissues. While this approach is sufficient for distinguishing low fat from high fat content, T1-weighting is not reliable when quantitative results and/or finer distinctions are required. A quantitative measure of bone marrow fat fraction is the Iterative Decomposition of Water and Fat with Echo Asymmetric and Least—Squares Estimation (IDEAL) imaging technique, which can be used to create parametric fat fraction maps, providing both quantitative and spatially resolved information on marrow composition (6-10). Liang et al. (11) showed that fat fraction maps have sufficient spatial resolution to be utilized in radiation therapy planning in patients undergoing pelvic chemoradiation.

Bolan et al. (12) showed that water-fat MRI could be used to assess changes in bone marrow fat content in patients with gynecologic malignancies pre- and post-chemotherapy and radiotherapy. These investigators showed chemotherapy-induced changes are uniform in space and radiation-induced changes are consistent with red to yellow marrow transformation. Although they showed an increase in marrow fat fraction at the L4 level from baseline to 6 months post-treatment, they did not provide quantitative data for other vertebrae. Further, they did not test differences in the magnitude, rate, and pattern of change between treatment groups or how fat fraction changes relate to clinically significant variables such as the development of neutropenia.

The primary aim of this study was to assess the magnitude, rate, and pattern of change in vertebrae bone marrow fat fraction for patients receiving highly myelotoxic versus less myelotoxic pelvic chemoradiotherapy and versus radiotherapy alone. The study's secondary aim was to determine associations between peripheral blood cell counts and fat fraction changes. Measuring composition changes over the course of treatment may provide

quantitative spatial evidence to support bone marrow-sparing treatment planning approaches.

METHODS AND MATERIALS

Study Design and Patients

This prospective, longitudinal, single-site clinical study was approved by the institutional review board and is compliant with the Health Insurance Portability and Accountability Act. The population comprised patients undergoing pelvic chemoradiotherapy or radiotherapy alone for gynecologic, ano-rectal, or genitourinary malignancies. Subjects treated with palliative intent were excluded. Subjects were recruited from the institution's radiation oncology clinics. All subjects provided informed consent. Our research budget allowed us to screen 27 subjects from November 2008 to July 2012, with 19 electing to participate (9 cervical cancer; 2 endometrial cancer; 3 anal cancer; 1 rectal cancer; 4 prostate cancer).

Treatment

All patients received intensity-modulated radiation therapy (IMRT). Four prostate cancer patients received pelvic radiotherapy only, 45.0 Gy in 1.8 Gy fractions to the pelvis, followed by a sequential boost to a total dose of 75.6-81.0 Gy. Two endometrial cancer patients underwent hysterectomy followed by adjuvant carboplatin (Area Under Curve = 6) and paclitaxel (175 mg/m^2 IV) for 6 cycles, followed by pelvic radiotherapy 45.0-50.4 Gy in 1.8 Gy fractions. Anal cancer patients received 45-58.2 Gy in 1.5-2.0 Gy fractions with either concurrent 5-FU (1000 mg/m^2 IV, on days 1-4 and 29-32) and mitomycin-C (10 mg/m^2 IV, on days 1 and 29) (2 patients) or cisplatin (75 mg/m^2 IV q 28 days × 2), 5-FU (1000 mg/m^2 IV on days 1-4 q 28 days × 2), and cetuximab (400 mg/m^2 loading, then 250 mg/m^2/wk. IV × 6-8 wks.) (1 patient). Nine cervical cancer patients received pelvic radiotherapy 45.0-50.4 Gy in 1.8 Gy fractions with concurrent cisplatin 40 mg/m^2 weekly, followed by high dose rate brachytherapy (30 Gy in 5 fractions to point A). One rectal cancer patient received pelvic radiotherapy 50.4 Gy in 1.8 Gy fractions with concurrent capecitabine (825 mg/m^2, twice daily for 5/days week). One of three anal cancer patients and one of two uterine cancer patients received pelvic-inguinal radiation. Two of nine cervical cancer patients received extended field (i.e., pelvic-paraaortic) radiotherapy. All patients completed chemoradiotherapy without treatment delays and no patients received granulocyte colony-stimulating factors.

For this study, we broadly classified treatment into two main categories: highly myelotoxic treatment and less myelotoxic treatment (Table 1). The highly myelotoxic treatment group consisted of cervical cancer patients treated with cisplatin and anal cancer patients treated with 5FU/MMC or cisplatin/5FU/cetuximab. The less myelotoxic treatment group comprised patients receiving no concurrent chemotherapy or concurrent capecitabine.

Concurrent Imaging and Laboratory Blood Tests

Patients underwent MRI with quantitative IDEAL (IDEAL-IQ) at baseline (within a 30 day window), mid-treatment (within a 14 day window), and post-treatment (within 30 days of completion). MRI scans were performed on a 3.0T scanner (Signa HDx, GE Healthcare,

Milwaukee, WI). A spine phased array coil was used. The IDEAL-IQ sequence is a multiple echo 3D SPGR with typical TR 10 ms, flip angle 3° and 6 echo times between 1.0 and 6.0 ms. The technique estimates fat fraction and R2* with corrections included for B0 inhomogeneity, fat spectrum, and noise bias. Sagittal spinal scans were obtained with each study. White blood cell counts (WBC) and absolute neutrophil counts (ANC) were collected at baseline and weekly for patients undergoing chemoradiotherapy. Prostate cancer patients did not undergo serial blood count measurements. Peripheral blood counts obtained closest to the time of each MRI acquisition (within a 7 day window) were used for the analysis.

Image Analysis and Dose Calculation

A two-dimensional region of interest (ROI) was drawn at the center of each subject's vertebrae (C3-S2) from serial sagittal spine MRIs using the Osirix DICOM viewer (version 4.1) (13). Each ROI contained approximately 100-200 voxels. The vertebral ROIs were positioned to include vertebral body bone marrow and avoid areas of partial volume and image artifact. Each ROI was inspected and manually adjusted, if necessary, to account for subject motion between scans. The mean signal intensity within the ROI provided corresponding vertebrae marrow proton density fat fraction (PDFF) values. PDFF in a given sample is defined as the number of protons in fat (triglycerides) divided by the total number of protons (water plus fat) expressed as percentages from 0 to 100 (6). ROIs were grouped into three vertebral column regions: L4-S2 (area consistently receiving large doses within pelvic field), T10-L3 (area superior to pelvic field receiving variable doses), and C3-T9 (area receiving no dose). Grand mean PDFF(%) values (which we refer to as PDFF(%)) were calculated for each subject according to region. From the radiation treatment plans, cumulative mean doses (in Gy) were calculated for each subject according to region at mid and post-treatment visits.

Statistical Analysis

Student's t, Mann-Whitney U, and Fisher's exact tests were used to analyze baseline differences in age, race, sex, body mass index (BMI), WBC, and ANC between the highly myelotoxic and less myelotoxic treatment groups. To estimate the effects of myelotoxic chemotherapy on fat fraction, we performed linear mixed effects (LME) modeling of the mean PDFF(%), with fixed interaction and main effects terms for chemotherapy (highly myelotoxic vs. less myelotoxic), cumulative mean dose (continuous, Gy), time (continuous), and location within the vertebral spine (L4-S2 vs. T10-L3 vs. C3-T9) (14,15). Akaike's information criterion (AIC) based on the maximum likelihood (ML) was used to select the linear-time model versus a profile-time model. Model parameter estimation was based on restricted maximum likelihood (REML) (16). To control for correlated observations within subjects, we created a subject-specific random slope for time and included it in the LME model. We tested the effects of potential confounders: age (continuous, mean centered), and whether subjects received pre-treatment chemotherapy (yes vs. no). Due to the risk of model over-fitting, we did not test the effects of other potential confounders, such as BMI. All possible secondary and tertiary interaction terms were tested. Forward and backward elimination was performed and main effects and interaction terms were significant at $p \leq .20$ and $p \leq .05$, respectively.

To test associations between peripheral blood cell counts and bone marrow fat fraction, we performed Spearman rank correlations for the difference in mean proton density fat fraction (ΔPDFF(%)) between the end of treatment (t_2) and baseline (t_0) vs. -log(WBC_{t2}/WBC_{t0}), -log(ANC_{t2}/ANC_{t0}), and WBC and ANC nadirs (lowest values occurring during radiotherapy). Rank correlation statistics were computed overall and according to vertebral column region. All tests were two-tailed with significant correlations at $p \leq .05$. Data were prepared and analyzed in R version 2.15.1 (http://www.r-project.org).

RESULTS

Twelve patients received highly myelotoxic treatment and seven patients received less myelotoxic treatment (Table 1). The median age was 55 (range: 27-81) years. Patients were younger in the highly myelotoxic treatment group. There was no difference in race, BMI, WBC, and ANC between treatment groups.

Fifteen of nineteen patients completed all three IDEAL IQ scans (baseline, mid-treatment, and post-treatment. Two patients completed only the baseline and mid-treatment scans, one patient completed only the baseline and post-treatment scan, and one patient completed only the mid-treatment and post-treatment scan. Altogether, 18, 18, and 17 patients completed the baseline, mid-treatment, and post-treatment scans, respectively. The mean (±standard deviation (SD)) number of days from the baseline IDEAL-IQ scan to the mid-treatment and post-treatment scans were 24 (±10) and 55 (±13) days, respectively.

Twelve patients completed all three WBC draws (baseline, mid-treatment, and post-treatment). Two patients completed only the baseline and mid-treatment WBC, one patient completed only the baseline and post-treatment WBC, and one patient completed only the baseline WBC. Altogether, 16, 14, and 13 patients completed the baseline, mid-treatment, and post-treatment WBC measurements, respectively. The mean (±standard deviation (SD)) number of days for the WBC measurements relative to the baseline, mid-treatment, and post-treatment MRI scans were 2 (±5), -1 (±3), and 1 (±6) days, respectively.

Nine patients completed all three ANC draws (baseline, mid-treatment, and post-treatment). Two patients completed only the baseline and mid-treatment ANC, one patient completed only the baseline and post-treatment ANC, one patient completed only the mid-treatment and post-treatment ANC, and one patient completed only the baseline ANC. Altogether, 14, 12, and 11 patients completed the baseline, mid-treatment, and post-treatment WBC measurements, respectively. The mean (±standard deviation (SD)) number of days for the WBC measurements relative to the baseline, mid-treatment, and post-treatment MRI scans were 1 (±5), -1 (±3), and 1 (±6) days, respectively.

Mean PDFF(%) values and cumulative mean doses are shown in Table 2. At baseline, mean PDFF(%) was significantly lower in the highly myelotoxic treatment group compared to the less myelotoxic treatment group (37.5% vs. 53.6%, $p<.001$), likely due to the fact that some patients in the low myelotoxic group received pre-treatment chemotherapy. Fig. 1 shows a representative image from a subject who received highly myelotoxic chemoradiotherapy (Fig. 1 A-C) compared to a subject who received radiotherapy alone (Fig. 1 D-F). Images

were produced at baseline, at mid treatment, and upon completion of treatment. Qualitatively, images A-C appear to have higher increases in fat fraction during treatment compared to images D-F. To help readers differentiate the signal intensities, we present PDFF(%) values for L5 ROI's: for the subject receiving highly myelotoxic treatment, L5 progressively increases during treatment (59.4% to 78.5% to 92.1%), and for the subject receiving only radiotherapy, L5 slightly increases but then decreases at the end treatment (59.5% to 65.8% to 63.8%).

Fig. 2 depicts mean differences in PDFF(%) for regions (A) T10-L3 and (B) L4-S2 relative to the reference (C3-T9) by group and visit. At baseline, the relative differences in PDFF(%) for both regions are higher for the less myelotoxic group. However, over the course of treatment we observe greater differences in PDFF(%) within both regions in the highly myelotoxic group compared to the less myelotoxic group.

Table 3 shows adjusted mean PDFF(%) estimates by MRI study visit, treatment group, vertebral column region and confounders with less myelotoxic treatment as the reference group. In the less myelotoxic group, we observed significant increases in mean PDFF(%) within T10-L3 and L4-S2 relative to C3-T9 (intercept). When we performed the analysis with highly myelotoxic treatment as the reference group, we also observed significant increases in mean PDFF(%) within T10-L3 (4.48%, 95%CI: 0.63%, 8.32%, p=.02) and L4-S2 (11.6%, 95% CI: 7.73%, 15.5%, p<.001) relative to C3-T9 (34.5%, 95%CI: 2.78%, 41.2%, p<.001). The adjusted model showed no significant differences between treatment groups for each region at baseline. Similarly, we observed no differences when we excluded patients who received pre-treatment chemotherapy. Pre-treatment chemotherapy was associated with an increase in baseline PDFF(%) of 12.8% (95%CI: -2.70%, 28.2%) and age was associated with an increase in PDFF(%) of 0.39% per year (95%CI: 5.6e-4%, 0.79%). We observed a significant effect of cumulative mean dose on the mean PDFF(%) (0.43% per Gy, 95%CI: 0.13%, 0.72%). In the less myelotoxic group, we observed no significant differences in the change in mean PDFF(%) per visit according to region. With highly myelotoxic treatment as the reference group, we observed significant differences in the change in mean PDFF(%) per visit according to T10-L3 (3.93% per visit, 95% CI: 0.90, 6.96, p=.01) and L4-S2 (10.1% per visit, 95% CI: 5.01, 15.2, p<.001) relative to C3-T9. These effects were still present when we excluded patients who received extended field radiotherapy (T10-L3: 3.44% per visit, 95% CI: 0.12%, 6.77%, p=.04; L4-S2: 9.06% per visit, 95% CI: 2.50%, 15.6%, p=.006). For the highly myelotoxic group relative to the less myelotoxic group, we observed a significant difference in the change in PDFF(%) per visit within L4-S2 (5.36% per visit, 95% CI: 0.29%,10.4%). We did not observe significant differences between treatment groups for C3-T9 or T10-L3 regions. Of note, when we did not control for region, we also observed a significant difference in the change in PDFF(%) per visit within C3-S2 (4.58% per visit, 95% CI: 0.52%, 8.64%, p=.03).

Fig. 3 depicts scatterplots and Spearman rank correlations for ΔPDFF(%) versus peripheral blood cell counts for C3-S2 (Fig. 3A) and by each vertebral region (Fig. 3B-D). Significant positive correlations were observed between ΔPDFF(%) and $-\log(WBC_{t2}/WBC_{t0})$ for T10-L3 (r=0.69, p=.02), L4-S2 (r=0.78, p=.004), and C3-S2 (r=0.76, p=.006), indicating that increasing fat fraction correlates with decreasing WBC counts over the course of treatment.

Similarly, significant correlations were observed between ΔPDFF(%) and -log(ANC_{t2}/ANC_{t0}) for L4-S2 (r=0.81, *p*=.008) and C3-S2 (r=0.79, *p*=.01), and was borderline for T10-L3 (r=0.62, *p*=.06). No significant correlations between ΔPDFF(%) and -log(WBC_{t2}/WBC_{t0}) or –log(ANC_{t2}/ANC_{t0}) were observed within C3-T9.

We also observed significant negative correlations between ΔPDFF(%) and WBC nadirs within C3-S2 (r=-0.57, *p*=.03) and T10-L3 (r=-0.69, *p*=.006), and a borderline significant correlation for L4-S2 (r=-0.49, *p*=.07), indicating an association between increased fat fraction and lower blood count nadirs. Similarly, we observed borderline significant negative correlations between ΔPDFF(%) and ANC nadirs within C3-S2 (r=-0.50, *p*=.10), T10-L3 (r=-0.52, *p*=.08), and L4-S2 (r=-0.51, *p*=.09). No significant correlations between ΔPDFF(%) and WBC and ANC nadirs were observed within C3-T9.

DISCUSSION

Multiple studies indicate that increased radiation dose to pelvic bone marrow is associated with greater hematologic toxicity in patients undergoing chemoradiotherapy (11,17-25). Modern radiotherapy techniques can allow the incorporation of functional bone marrow imaging to specifically avoid hematopoietically active marrow subregions, which may reduce hematologic toxicity and increase chemotherapy tolerance (18,24,26).

In this study, we used IDEAL-IQ to compare changes in vertebral bone marrow fat fraction in patients undergoing highly myelotoxic chemoradiotherapy versus less myelotoxic chemoradiotherapy or radiotherapy alone. Overall, we observed that cumulative mean dose leads to significant increases in PDFF(%) within the vertebral bone marrow. These changes in PDFF(%) also corresponded to decreasing peripheral blood cell counts. In the highly myelotoxic group, we observed significant increases in PDFF(%) over the course of treatment within (i.e., L4-S2) and above the pelvic radiation field (i.e., T10-L3), even in patients who did not undergo extended field radiotherapy. PDFF(%) increases within the pelvic radiation field were significantly more pronounced in the highly myelotoxic group relative to the less myelotoxic group. Altogether these findings suggest that IDEAL is sensitive to marrow composition changes resulting from chemotherapy and radiation, and that locoregional radiation effects contribute to the manifestation of clinical myelosuppression, particularly in patients undergoing myelotoxic chemotherapy.

Although conventional MR imaging may broadly distinguish red and yellow bone marrow (27), quantifying subtle gradations within red marrow in response to radiotherapy is possible only using recent advances in MR fat quantification methodology (6,12,28-31). The use of MR with fat quantification allows non-invasive monitoring of the spatial effects of radiotherapy, and to quantify the degree of red marrow damage as a function of radiation dose. This allows us to model and estimate the impact of conformal radiation techniques on red bone marrow injury.

This study had several limitations. There is significant heterogeneity in the population. To a degree, this heterogeneity was useful to estimate the impact of varying conditions on changes in marrow fat composition; however, further studies are ongoing in more

homogeneous populations to control effects of treatment and demographic factors that could influence our findings (32). This longitudinal study included a relatively small sample and was subject to dropout, reducing our statistical power. Although we do not suspect this would have biased our primary effect estimates, this may have limited our ability to detect significant differences in the effects of chemotherapy in regions superior to the pelvic field. Our model form does assume a linear rate of change in fat fraction according to treatment group and spatial location, which may or may not be valid. However, the linear time model has the advantage of simplicity and parsimony, and appeared to model the data well.

In summary, we observed increases in bone marrow fat composition over the course of treatment occurring specifically within the radiation treatment field, particularly in the presence of concurrent myelotoxic chemotherapy. These findings indicate that locoregional effects of radiation therapy likely significantly contribute to the clinical manifestation of myelosuppression in this setting. Modern radiotherapy techniques specifically designed to spare functioning bone marrow may reduce myelosuppression and permit better tolerance to myelotoxic chemotherapy regimens.

Acknowledgments

This research was funded by the National Cancer Institute (1R21CA162718-01) and GE Healthcare (Pittsburgh, PA).

REFERENCES

1. Sacks EL, Goris ML, Glatstein E, Gilbert E, Kaplan HS. Bone marrow regeneration following large field radiation: influence of volume, age, dose, and time. Cancer. 1978; 42:1057–1065. [PubMed: 100197]
2. Georgiou KR, Foster BK, Xian CJ. Damage and recovery of the bone marrow microenvironment induced by cancer chemotherapy — potential regulatory role of chemokine CXCL12/receptor CXCR4 signaling. Curr Mol Med. 2010; 10:440–453. [PubMed: 20540706]
3. Blankenberg FG. In vivo detection of apoptosis. J Nucl Med. 2008; 49:81S. [PubMed: 18523067]
4. Crawford J, Dale DC, Lyman GH. Chemotherapy-induced neutropenia: risks, consequences, and new directions for its management. Cancer. 2004; 100:228–237. [PubMed: 14716755]
5. Elting LS, Rubenstein EB, Martin CG, et al. Incidence, cost, and outcomes of bleeding and chemotherapy dose modification among solid tumor patients with chemotherapy-induced thrombocytopenia. J Clin Oncol. 2001; 19:1137–1146. [PubMed: 11181679]
6. Reeder SB, Pineda AR, Wen Z, et al. Iterative decomposition of water and fat with echo asymmetry and least-squares estimation (IDEAL): application with fast spin-echo imaging. Magn Reson Med. 2005; 54:636–644. [PubMed: 16092103]
7. Rosen BR, Fleming DM, Kushner DC, et al. Hematologic bone marrow disorders: quantitative chemical shift MR imaging. Radiology. 1988; 169:799–804. [PubMed: 3187003]
8. Johnson LA, Hoppel BE, Gerard EL, et al. Quantitative chemical shift imaging of vertebral bone marrow in patients with Gaucher disease. Radiology. 1992; 182:451–455. [PubMed: 1732964]
9. Brix G, Heiland S, Bellemann ME, Koch T, Lorenz WJ. MR imaging of fat-containing tissues: valuation of two quantitative imaging techniques in comparison with localized proton spectroscopy. Magn Reson Imaging. 1993; 11:977–991. [PubMed: 8231682]
10. Liney GP, Bernard CP, Manton DJ, Turnbull LW, Langton CM. Age, gender, and skeletal variation in bone marrow composition: a preliminary study at 3.0 Tesla. J Magn Reson Imaging. 2007; 26:787–793. [PubMed: 17729356]

11. Liang Y, Bydder M, Yashar CM, et al. Prospective study of functional bone marrow-sparing intensity modulated radiation therapy with concurrent chemotherapy for pelvic malignancies. Int J Radiat Oncol Biol Phys. 2013; 85:406–414. [PubMed: 22687195]
12. Bolan PJ, Arentsen L, Sueblinvong T, et al. Water-Fat MRI for assessing changes in bone marrow composition due to radiation and chemotherapy in gynecologic cancer patients. J Magn Reson Imaging. 2013; 38:1578–1584. [PubMed: 23450703]
13. Rosset A, Spadola L, Ratib O. OsiriX: open-source software for navigating in multidimensional DICOM images. J Digital Imaging. 2004; 17:205–216.
14. Pinheiro, J.; Bates, D.; DebRoy, S.; Sarkar, D.; the R Development Core Team. nlme: Linear and Nonlinear Mixed Effects Models.. R package version 3.1-104. 2012.
15. Laird NM, Ware JH. Random-Effects Models for Longitudinal Data. Biometrics. 1982; 38:963–974. [PubMed: 7168798]
16. Gilmour AR, Thompson R, Cullis BR. Average Information REML: An Efficient Algorithm for Variance Parameter Estimation in Linear Mixed Models. Biometrics. 1995; 51:1440–1450.
17. Mell LK, Kochanski JD, Roeske JC, et al. Dosimetric predictors of acute hematologic toxicity in cervical cancer patients treated with concurrent cisplatin and intensity-modulated pelvic radiotherapy. Int J Radiat Oncol Biol Phys. 2006; 66:1356–1365. [PubMed: 16757127]
18. Mell LK, Schomas DA, Salama JK, et al. Association between bone marrow dosimetric parameters and acute hematologic toxicity in anal cancer patients treated with concurrent chemotherapy and intensity-modulated radiotherapy. Int J Radiat Oncol Biol Phys. 2008; 70:1431–1437. [PubMed: 17996390]
19. Rose BS, Aydogan B, Liang Y, et al. Normal tissue complication probability modeling of acute hematologic toxicity in cervical cancer patients treated with chemoradiotherapy. Int J Radiat Oncol Biol Phys. 2011; 79:800–807. [PubMed: 20400238]
20. Rose BS, Liang Y, Lau SK, et al. Correlation between radiation dose to [chk]^{1}□ F-FDG-PET defined active bone marrow subregions and acute hematologic toxicity in cervical cancer patients treated with chemoradiotherapy. Int J Radiat Oncol Biol Phys. 2012; 83:1185–1191. [PubMed: 22270171]
21. Liang Y, Messer K, Rose BS, et al. Impact of bone marrow radiation dose on acute hematologic toxicity in cervical cancer: principal component analysis on high dimensional data. Int J Radiat Oncol Biol Phys. 2010; 78:912–919. [PubMed: 20472344]
22. Klopp AH, Moughan J, Portelance L, et al. Hematologic toxicity in RTOG 0418: a phase 2 study of postoperative IMRT for gynecologic cancer. Int J Radiat Oncol Biol Phys. 2013; 86:83–90. [PubMed: 23582248]
23. Bazan JG, Luxton G, Mok EC, Koong AC, Chang DT. Normal tissue complication probability modeling of acute hematologic toxicity in patients treated with intensity-modulated radiation therapy for squamous cell carcinoma of the anal canal. Int J Radiat Oncol Biol Phys. 2012; 84:700–706. [PubMed: 22414279]
24. McGuire SM, Menda Y, Ponto LL, et al. A methodology for incorporating functional bone marrow sparing in IMRT planning for pelvic radiation therapy. Radiother Oncol. 2011; 99:49–54. [PubMed: 21397965]
25. Bazan JG, Luxton G, Kozak MM, et al. Impact of Chemotherapy on Normal Tissue Complication Probability Models of Acute Hematologic Toxicity in Patients Receiving Pelvic Intensity Modulated Radiation Therapy. Int J Radiat Oncol Biol Phys. 2013; 87:983–991. [PubMed: 24161422]
26. Liang Y, Kim GY, Pawlicki T, Mundt AJ, Mell LK. Feasibility study on dosimetry verification of volumetric-modulated arc therapy-based total marrow irradiation. J Appl Clin Med Phys. 2013; 14:3852. [PubMed: 23470926]
27. Blomlie V, Rofstad EK, Skjønsberg A, et al. Female Pelvic Bone Marrow: Serial MR Imaging before, during, and after Radiation Therapy. Radiology. 1995; 194:537–543. [PubMed: 7824737]
28. Liu C-Y, McKenzie CA, Yu H, Brittain JH, Reeder SB. Fat quanti- fication with IDEAL gradient echo imaging: correction of bias from T(1) and noise. Magn Reson Med. 2007; 58:354–364. [PubMed: 17654578]

29. Bydder M, Yokoo T, Hamilton G, et al. Relaxation effects in the quantification of fat using gradient echo imaging. Magn Reson Imaging. 2008; 26:347–359. [PubMed: 18093781]

30. Yu H, McKenzie CA, Shimakawa A, et al. Multiecho reconstruc- tion for simultaneous water-fat decomposition and T2* estima- tion. J Magn Reson Imaging. 2007; 26:1153–1161. [PubMed: 17896369]

31. Chebrolu VV, Hines CDG, Yu H, et al. Independent estimation of T^*_2 for water and fat for improved accuracy of fat quantification. Magn Reson Med. 2010; 63:849–857. [PubMed: 20373385]

32. Mell LK. Intensity modulated radiation therapy for gynecologic malignancies: a testable hypothesis. Int J Radiat Oncol Biol Phys. 2012; 84:566–568. [PubMed: 22999264]

SUMMARY

MRI fat quantification is sensitive to vertebrae bone marrow composition changes that result from chemoradiotherapy. These findings indicate that locoregional effects of chemoradiation likely contribute to the clinical manifestation of myelosuppression.

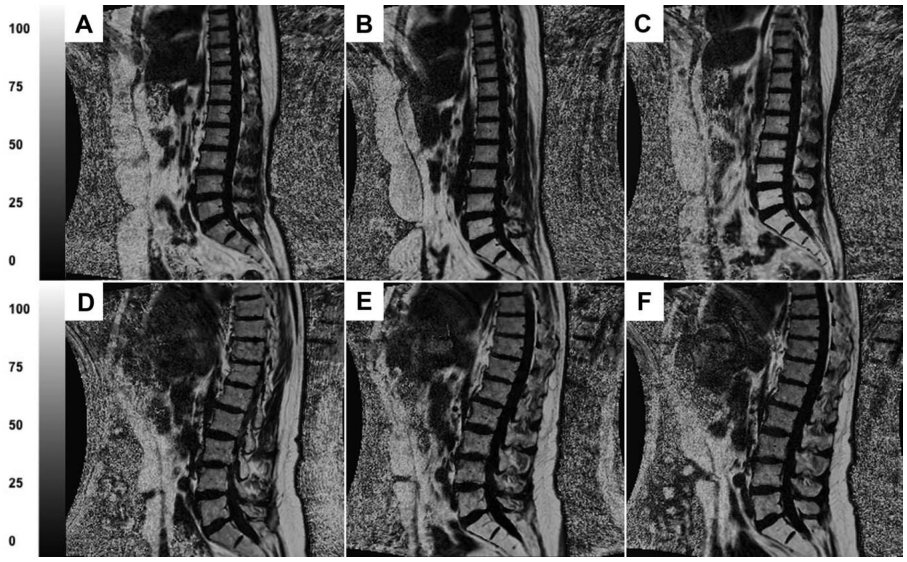

Fig. 1.

A-C represent MRIs from a subject with cervical cancer who received cisplatin chemotherapy and IMRT. D-F represent MRIs from a subject with prostate cancer who received IMRT alone. A and D were produced at baseline, B and E were produced at mid treatment, and C and F were produced immediately after treatment. PDFF(%) values for L5 regions of interest are: (A) 59.4%, (B) 78.5%, (C) 92.1%, (D) 59.5%, (E) 65.8%, and (F) 63.8%.

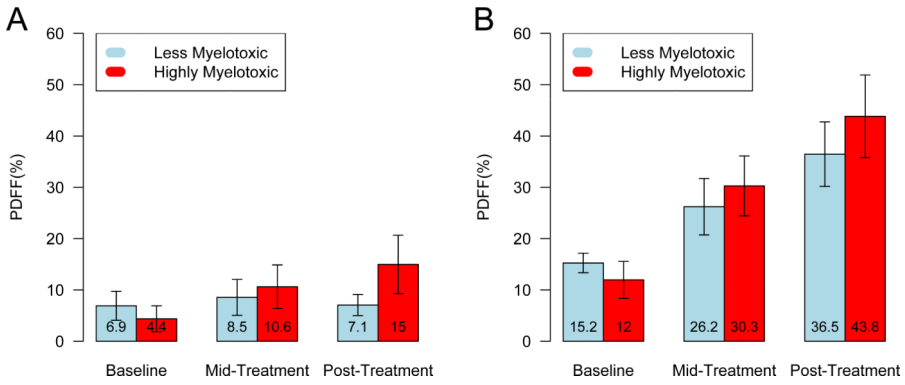

Fig. 2.

Bar plots of the mean difference (95% confidence intervals) in proton density fat fraction (PDFF(%)) for (A) T10-L3 and (B) L4-S2 relative to C3-T9, by treatment group and visit. PDFF(%) values are labeled within bars.

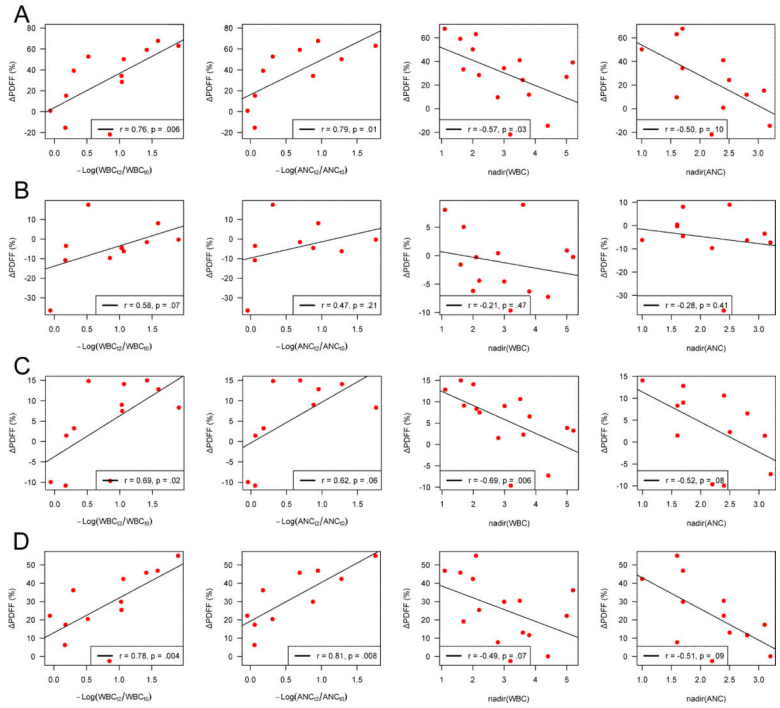

Fig. 3.

Scatterplots and Spearman rank correlations for the difference in PDFF(%) versus peripheral blood cell counts by (**A**) C3-S2, (**B**) C3-T9, (**C**) T10-L3, and (**D**) L4-S2.

Table 1

Patient, Tumor and Treatment Characteristics

Characteristic	Highly Myelotoxic	Less Myelotoxic	All	*p*
Number of Patients, n	12	7	19	
Age (SD), years	48 (13)	62 (7)	53 (13)	.006
Women, n (%)	10 (83°%)	3 (43%)	13	.17
Race, n (%)				.34
Caucasian	7 (58%)	6 (86%)	13	
Hispanic	4 (33%)	0 (0%)	4	
Asian	1 (8%)	1 (14%)	2	
BMI (SD), kg/m^2	26.2 (6)	26.3 (6.1)	26.2 (5.8)	.99
Cancer Site: Stage (n)	Cervix: IBI (4), IB2 (2), IIB2 (2), IIIB (1); Anus: IIIA (3)	Uterus: IIIB (1), IV (1); Rectum: IIIA (1); Prostate: III (4)	Cervix: 9; Uterus: 2; Anus: 3; Rectum: 1; Prostate: 4	
Chemotherapy (n)	CDDP (9) 5FU/MMC (2) CDDP/5FU/Cetuximab (1)	CAP (1) No concurrent chemo (6)	CDDP (9); 5FU/MMC (2) CDDP/5FU/Cetuximab (1) CAP (1) No concurrent chemo (6)	
Pre-treatment chemo, n (%)	0 (0%)	3 (43%)	3	.04
IMRT, n (%)	12 (100%)	7 (100%)	19	1.0
Pelvic-aortic RT, n (%)	2 (17%)	0 (0%)	2	.51
Pelvic-inguinal RT, n (%)	1 (8%)	1 (14%)	2	1.0
WBC × $10^3/\mu$ (SD)	7.25 (2.5)	6.3 (0.5)	16	.58
ANC × $10^3/\mu$ (SD)	4.6 (1.9)	3.7 (0.4)	14	.22

Abbreviations: SD = standard deviation; BMI = body mass index; chemo = chemotherapy; CDDP = cisplatin; 5FU = 5-fluorouracil; MMC = mytomycin C; CAP = capecitabine; IMRT = intensity modulated radiotherapy; RT = radiotherapy; WBC = white blood cell count; ANC = absolute neutrophil count.

Table 2

Mean Proton Density Fat Fraction, % (SD) and Cumulative Mean Dose, Gy (SD) by MRI Study Visit, Treatment Group and Vertebral Column Region

		Baseline		Mid-Treatment		Post-Treatment	
Treatment Group	**Region**	**PDFF(%)**	**Cum. Dose**	**PDFF(%)**	**Cum. Dose**	**PDFF(%)**	**Cum. Dose**
Highly Myelotoxic	C3-T9	33.0 (11.1)	0	34.9 (11.5)	0	30.5 (15.5)	0
	T10-L3	36.0 (13.9)	0	41.2 (14.1)	0.42 (0.78)	42.0 (18.7)	0.60 (1.07)
	L4-S2	43.2 (16.5)	0	64.3 (15.5)	19.3 (5.85)	74.1 (15.5)	28.3 (5.37)
	All Vertebrae (C3-S2)	37.5 (14.4)	0	46.5 (18.3)	6.77 (9.79)	49.7 (23.7)	9.93 (13.9)
Less Myelotoxic	C3-T9	47.2 (11.5)	0	48.0 (11.0)	0	41.4 (11.3)	0
	T10-L3	52.6 (12.8)	0	51.8 (13.4)	0.17 (0.11)	47.9 (11.7)	0.28 (0.09)
	L4-S2	61.6 (11.2)	0	70.3 (14.2)	18.9 (7.68)	77.8 (12.7)	28.0 (3.86)
	All Vertebrae (C3-S2)	53.6 (13.1)	0	57.1 (15.3)	6.67 (10.2)	55.8 (18.9)	9.41 (13.7)

Abbreviations: SD = standard deviation; C = cervical vertebrae; T = thoracic vertebrae; L = lumbar vertebrae; S = sacral vertebrae; PDFF(%) = proton density fat fraction; Cum. Dose = cumulative mean dose (in Gy)

Table 3

Adjusted Mean Proton Density Fat Fraction (%) Estimates and 95% CI by MRI Study Visit, Treatment Group, Vertebral Column Region and Confounders

	Parameter	Mean PDFF(%)	*p*
Baseline estimates for the less myelotoxic group	C3-T9 (intercept)	37.3 (25.7,49.0)	<.001
	T10-L3	+5.94 (0.71,11.2)	.02
	L4-S2	+13.9 (8.68,19.2)	<.001
Difference in estimates for the highly myelotoxic group relative to the less myelotoxic group at baseline	C3-T9	−2.83 (−18.2,12.5)	.70*
	T10-L3	−1.45 (−7.95,5.03)	.66*
	L4-S2	−2.33 (−8.82,4.16)	.48*
Change in PDFF(%) per visit for the Less myelotoxic group	C3-T9	+1.84 (−6.03,2.34)	.38
	T10-L3	+0.37 (−3.69,4.44)	.86
	L4-S2	+4.76 (−1.00,10.5)	.10
Difference in the change in PDFF(%) per visit between the highly myelotoxic and less myelotoxic groups	C3-T9	+1.50 (−3.74,6.73)	.57†
	T10-L3	+3.56 (−1.51,8.63)	.16†
	L4-S2	+5.36 (0.29,10.4)	.04†
	Cum. Dose (per Gy)	+0.43 (0.13,0.72)	.004
	Pre-treatment chemo	+12.8 (−2.70,28.2)	.08
	Age (per year)	+0.39 (5.6e-4,0.79)	.05

Abbreviations: PDFF(%) = proton density fat fraction (%); CI = confidence interval; C = cervical vertebra; T = thoracic vertebra; L = lumbar vertebra; S = sacral vertebrae; chemo = chemotherapy; Cum. Dose = cumulative mean dose (in Gy).

* *p*-value is testing the difference in mean PDFF(%) for the highly myelotoxic group relative to the less myelotoxic group at baseline by vertebral column region.

† *p*-value is testing the difference in the change in mean PDFF(%) per visit for the highly myelotoxic group relative to the less myelotoxic group by vertebral column region.